Photocatalytic Degradation of Industrial Dye in Semi-Pilot Scale Prototype Solar Photoreactor: Optimization and Modeling Using ANN and RSM Based on Box-Wilson Approach

M. Berkani, M. K. Bouchareb, M. Bouhelassa, Yassine Kadmi

Topics in Catalysis (2020) 63:964–975
https://doi.org/10.1007/s11244-020-01320-0

ORIGINAL PAPER

Photocatalytic Degradation of Industrial Dye in Semi-Pilot Scale Prototype Solar Photoreactor: Optimization and Modeling Using ANN and RSM Based on Box–Wilson Approach

Mohammed Berkani[1] · Mohammed Kheireddine Bouchareb[2] · Mohammed Bouhelassa[2] · Yassine Kadmi[3,4]

Published online: 11 July 2020

Abstract
Photodegradation of an industrial Azo dye C.I Basic Red 46, was examined in a semi-pilot scale prototype solar photoreactor under solar radiation. In our study, photodegradation of the dye was optimized using Response Surface Methodology (RSM) based on Box-Wilson approach. The Artificial Neural Network (ANN) was used to establish suitable modeling and optimal conditions for the Solar UV/Immobilized-TiO_2 process in order to evaluate the individual effects of three factors that independently affect the effectiveness of the photodegradation process: (1) initial concentration of the dye, (2) pH, and (3) flow rate. The RSM was in good agreement with the prediction model ($R^2_{Dec} = 0.95$); meanwhile, the ANN approach revealed that the predicated model fit perfectly with the experimental data to yield the highest value of $R^2 = 0.999$. The effects of these three factors could be estimated from a second-order polynomial equation, and the optimal parameters of photodegradation consisted of three main parameters: (1) initial concentration of colorant 10.65 mg.L^{-1}, (2) pH 10.82, and (3) rate of fluid flow of 852 L h^{-1}. The decolorization removal efficiency under these optimal conditions was 99%.

Keywords Photocatalysis · Azo dye · Optimization · Response surface methodology · Artificial neural network · central composite design

1 Introduction

Organic dyes are widely used in various industries and generate around one trillion dollars, contribute to 7% of the total world exports. Organic dye industries, such those involving textiles, pharmaceuticals, colors, papers, cosmetics, photography, and food, employ around 35 million workers worldwide [1]. More than 0.7 million tons of organic synthetic dyes are produced annually worldwide. In addition, over 10,000 different dyes and pigments are applied in these industries [2].

The Danish Environmental Protection Agency (DEPA) has classified the azo-dye as a suspected human carcinogen and has suggested a maximum of 3.1 µg L^{-1} in drinking water for safety reasons [3]. Moreover, a recent study by the Occupational Dermatology Research Center in Australia recommended that the textile dye BR 46 be tested as a causative agent in cases of foot dermatitis [4].

Advanced oxidation processes (AOPs) are promising techniques that can be used as efficient processes for wastewater treatment of industrial textile dyes. Over the last several decades, AOPs have come under extensive scrutiny by many researchers due to the possibility of complete mineralization of the most toxic pollutants [2, 5, 6]. Heterogeneous photocatalysis, as one of the AOPs, has attracted much attention because these processes occur in the presence of irradiating sources in addition to a semiconductor with oxygen as a critical electron scavenger. Photocatalysis is a chemical

Electronic supplementary material The online version of this article (https://doi.org/10.1007/s11244-020-01320-0) contains supplementary material, which is available to authorized users.

✉ Mohammed Berkani
m.berkani@ensbiotech.edu.dz

[1] Laboratoire Biotechnologies, Ecole Nationale Supérieure de Biotechnologie, Ville Universitaire Ali Mendjeli, BP E66, 25100 Constantine, Algeria

[2] Laboratoire D'Ingénierie Des Procédés de L'Environnement, Faculté Génie Des procédés, Université de Constantine 3, Route Ain el bey, 25000 Constantine, Algeria

[3] LASIRE CNRS UMR 8516, Sciences et Technologies, Université Lille, 59655 Villeneuve d'Ascq Cedex, France

[4] IUT de Béthune, Université d'Artois, 62400 Béthune, France

reaction that occurs via photon absorption by a solid material, known as a photocatalyst. Thus, based on photocatalytic activity, the photonic excitation of a photocatalyst (semiconductor) generates electron–hole pairs in its surface, and the photocatalysis process can be recapitulated in water in five steps: (1) transfer to the surface of photocatalysts, (2) adsorption of the reactants, (3) photonic activation of the photocatalyst, (4) desorption, and (5) finally, elimination of reaction products from the interface region.

The highly oxidative h^+_{vB} can react with surface bound H_2O to produce hydroxyl radicals °OH or can directly react with the organic molecules [7, 8]:

$$Catalyst + h_v \rightarrow e^-_{CB} + h^+_{vB} \quad (1)$$

$$OH^-_{\text{ads}} + e^-_{CB} \rightarrow HO^{\bullet}_{\text{ads}} \quad (2)$$

$$H_2O_{ads} + h^+_{vB} \rightarrow HO^{\bullet}_{ads} + H^+ \quad (3)$$

$$O_2 + e^-_{CB} \rightarrow O^{\bullet}_2- \quad (4)$$

$$O^{\bullet}_2- + H^+ \rightarrow HO^{\bullet}_2 \quad (5)$$

Thus, solar energy has been regarded as one of the most promising renewable energy-generating processes in recent years, interest has focused on the design of new solar photocatalytic reactors [9, 10]. Thus, solar photocatalysis is a more interesting process that consists of using the 5% of ultraviolet (UV) radiation in the solar spectrum that is sufficient to activate the catalyst. This technique is considered a durable developmental perspective based on renewable energy and is very promising, especially for a country that receives lots of sunlight, such as Algeria. Since the emergence of photocatalysis, several semi-pilot photoreactors for the treatment of water have recently been developed [11–14].

The photocatalysis process is strongly dependent on various operational conditions, which require the development of experimental designs that allow for the study and optimization of their influence during the photodegradation process. The design of these types of experiments is a powerful tool and can be used to examine the effects of the selected factors on the response process. Response surface methodology (RSM) has been extensively applied to solve many optimization processes [15, 16], including photocatalysis process with titanium oxide (TiO_2)-supported or slurry/UV oxidation [17, 18] and ozone or electrochemical oxidation processes [19]. Many recent studies use artificial neural networks (ANN) as robust tools that can be applied to a set of raw experimental data to address a wide range of problems, such as a non-linear mathematical relationships between the input and output of the process. ANN is an information processing paradigm consisting of many interconnected neurons that was loosely inspired by the human brain [20]. The neuron is a processing element that takes a number of inputs, weighs them, sums them up, adds a bias, and uses the outcome as the argument for a single-valued function (transfer function), which results in the neuron's output [21]. Recently, the ANN technique has been widely used for AOP modeling [22, 23] and photocatalytic processes [24–27].

However, as far as we know, studies on the solar UV/TiO_2 semi-pilot scale systems modeling using RSM and ANN are very limited even non-existent in the literature. In this study, we examined optimization of three independents parameters: (1) initial dye concentration, (2) pH, and (3) flow rate by training a neural network. To estimate an RSM based on the Box–Wilson design of photocatalytic decolorization of an industrial cationic dye Basic Red 46 (BR46) in a semi-pilot solar photoreactor using the catalyst TiO_2 Degussa P25 from the TiO_2/Solar UV system. Furthermore, this study provides a way to optimize such a photoreactor and will enable application of this device as specific treatment for a real water sample obtained from Aurassienne Spinning and Blankets (SAFILCO) Company, Algeria, charged by the dye, C.I. Basic Red 46 to achieve optimal results.

2 Experimental

2.1 Chemicals and materials

The solar photocatalytic reactor used in our study was a tubular reactor compound parabolic collector (CPC) type (Fig. 1) [15]. The volume of wastewater to be treated in each experiment was 10 L. The solar reactor was operated in the batch mode (Fig. 1) and consisted of five UV-transparent borosilicate glass tubes (length: 1 m, external diameter: 30 mm, thickness: 1.4 mm) made in Germany (Schott–Rohrglas GmbH Company) and delivered by SOMIVER (E.N.A.V.A) Company, Algeria. These tubes were connected in series to a storage tank (40 L capacity) by plastic joints and mounted on CPC-type aluminum reflector, thus ensuring that the light reaching the surface of the tubes was homogeneous. The volume that was effectively irradiated was 3.2 L, and the volume of colored water to be treated was 10 L. A stirrer inside the tank ensured a homogeneous concentration of particles in the solution. The effluent was circulated via a centrifugal pump. A flow meter, fitted with a calibration curve, was placed between the pump outlet and reactor inlet. The reactor was oriented south and inclined at an angle of 36° (latitude at Constantine, Algeria) with respect to the horizontal; with this position, the annual collection of solar energy is maximized. Basic Red 46 (Table 1) used in this

Fig. 1 Experimental solar set up

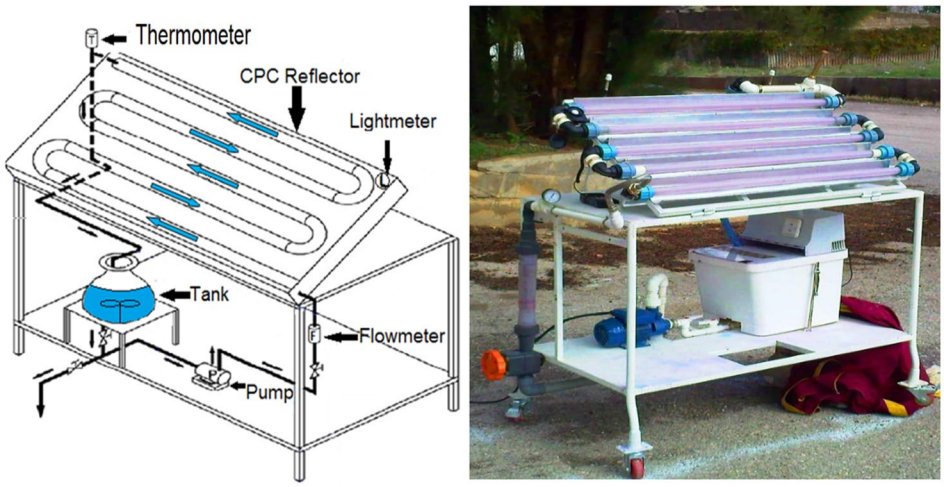

Table 1 Structure and characteristics of C.I.Basic Red 46

Structure	Class	C.I number	λ_{max}(nm)	Mw (g mol^{-1})
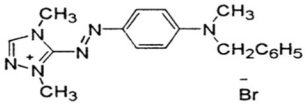	Cationic Mono-azo	110825	531	357.5

study is an industrial textile dye available at Aurassienne Spinning and Blankets (SAFILCO) Company, Algeria.

The photocatalyst used in our study was a commercial TiO_2 photocatalyst provided by Ahlstrom Company (France). The company produces paper with deposited TiO_2 used as flexible photocatalytic media. The immobilized catalysts consist of PC500 TiO_2 from Millennium Inorganic Chemicals (anatase: > 99%, specific surface area 350–400 $m^2\ g^{-1}$, crystallites mean size = 5–10 nm). In order to improve the adsorption capacity and the photocatalytic efficiency of the composition, the catalyst was coated onto nonwoven fibers (254 µm thickness) using an inorganic binder agent consisting exclusively of an aqueous colloidal dispersion of silicon dioxide (SiO_2). The SiO_2 represents from 20 to 50% by weight of the colloidal aqueous dispersion with 48% as the most advantageous weight (EP1069950B1 European patent). Moreover, to increase the specific surface area extender zeolite UOP (2000 $m^2\ g^{-1}$) was used to increase adsorption properties of the photocatalyst. Table 2 shows the physical and chemical characteristics. The presence of zeolite on the TiO_2 surface leads to an increase in surface area of the photocatalyst, which provides an effective way to create more reactive sites and better adsorption capacity and thus enhance photocatalytic activity. The scanning electron microscopy (SEM) image of TiO_2 nanoparticles deposited on non-woven paper and X-ray diffraction pattern (XRD) of TiO_2 PC-500 (Supplementary Data) reveal that the fiber surfaces show the agglomeration of the catalyst on the fiberglass cloth surface [28].

Table 2 Physico-Chemical properties of the immobilized photocatalyst

Compositions	
PC 500	18 g m^{-2}
SiO_2	20 g m^{-2}
UOP200	2 g m^{-2}
Physical properties	
Masse per unit area	75 g m^{-2}
Thickness	254 µm
Air permeability	2570 L m^{-2} s^{-2}
Tensile strength MD	1100 N m^{-2}
CD	500 N m^{-2}
Elongation MD	3%
CD	5%
Water drop	2%

The photocatalyst used in our study has also attracted the attention of several researchers, such as Ko [28, 29] who did a comparative study of the characterization of natural zeolite-based nano-titania composite sheets with non-woven photocatalytic paper purchased from Ahlstrom, (France, BR 1048- 075, 75 g m^{-2}).

2.2 Analytical procedures

All of the samples collected from the experiments were centrifuged at 4000 rpm for 25 min using a centrifuge (Sigma 2–16) to remove the TiO_2 nanoparticles. Color removal of dye BR46 was determined by UV absorption at $\lambda_{max} = 531$ nm using a UV–Vis spectrophotometer (Shimadzu UV-160A) and calibration curve based on Beer–Lambert's law; therefore, the photodegradation yield (Y%) can be explained by the ratio of residual concentration to the initial one as shown in Eq. 6:

$$Y = \frac{C_0 - C_i}{C_0} \times 100. \tag{6}$$

The percentage decolorization rate (Y, %) was expressed as the percentage ratio of decolorized dye concentration to that of the initial one. Y, C_0, and Ci are the decolorization efficiency (%) and the initial and decolorized dye concentrations, respectively. Solar radiation (400–720 nm) was measured with a light meter (Lutron; LX-107) mounted next to the CPCs.

The results of experiments are expressed as a function of accumulated solar energy Q_V (KJ L^{-1}) received by the reactor per unit volume of solution to be treated.

$$Q_{V,n} = Q_{V,n-1} + \Delta t_n \overline{V}_{G,n} \frac{A_r}{V_t} \tag{7}$$

$$\Delta t_n = t_n - T_{n-1}$$

in which $Q_{V,n}$ is the accumulated solar energy incident on the reactor (KJ L^{-1}), t_n is the experimental time of each sample, $V_{G,n}$ the solar radiation intensity (W m^{-2}) measured by the lightmeter, A_r is the collector surface (m^2), and V_t is the volume of solution to be treated (L). This dimension makes the comparison of degradation kinetics for different operating conditions possible regardless of the weather conditions and resulting solar irradiation. All experiments were conducted at at the temperature interval of 25–40 °C.

2.3 Experimental design

The second-order polynomial equation describes the rate of photodegradation versus the selected functional parameters, including initial dye concentration (X_1), pH (X_2), and flow rate (X_3), while the solar energy accumulated remained fixed at 60 kJ L^{-1} for all experiments. The photodegradation process was optimized applying the Central Composite Design (CCD) *or* Box–Wilson Design and RSM consisting, of 20 experiments. Table 3 represents the levels and ranges of the selected independent variables.

A second-order polynomial model was provided by the Box–Wilson design, which relates the response Y to the selected factors, X_1, X_2, X_3, was used to optimize the decolorization process:

Table 3 Range and levels of experimental parameters

Variable	Ranges and levels				
	− 1.68	− 1	0	+1	+1.68
X_1 $[RB46]_0$(mgL^{-1})	8.2	15	25	35	41.8
X_2 pH	2.8	4.5	7	9.5	11.2
X_3 Recirculation flow rate Q_L (Lh^{-1})	348	450	600	750	852

$$Y_{(\text{photodegradation efficiency})} = a_0 + a_1X_1 + a_2X_2 + a_3X_3 + a_{12}X_1X_2 + a_{13}X_1X_3 + a_{23}X_2X_3a_{11}X_1^2 + a_{22}X_2^2 + a_{33}X_3 \tag{8}$$

MINITAB stat software (17 Minitab Institute, USA) offers a full quadratic regression method to analyze responses, and this method was used to fit the mathematical experimental data models to the second-order polynomial equation.

2.4 Artificial neural network model development

The development of ANN models was studied using MATLAB 14a. Table 4 illustrates the different parameters. The feed-forward neural network with back propagation method is the most commonly encountered in physicochemical process modeling [29]. A three feed forward network with function "traingdx" was chosen as the training function, which describes the gradient decline with momentum and adaptive learning rate backpropagation, the input layer defined by three neurons that represents the dye concentration (mg L^{-1}), pH, and recirculation flow rate Q_L (L h^{-1}); on the other hand, the output layer comprises one (01) neuron as an interest rate such as BR46 degradation efficiency (%), as shown in Fig. 2.

The datasets were divided into three subsets in which 70% of the data was used for the training of the network, 15% for validation, and 15% for testing. The mean square error (MSE) was used to examine the relationship between the neurons in the hidden layer and network error or even more between the ANN model predictions and the experimental data as calculated by Eq. 9:

$$MSE = \sum_{i=1}^{N} \frac{(y_i - y_{i-pred})}{n} \tag{9}$$

and the coefficient of determination (R^2) was expressed as:

$$R^2 = \frac{\sum_{i=1}^{N} (y_i - y_{i-pred})^2}{\sum (y_{i-moy} - y_{i-pred})^2} \tag{10}$$

Table 4 ANN Parameters setting

Parameters	Condition
Input Neurons	Three (Dye concentration, pH, Recirculation flow rate)
Output Neurons	One (BR 46 Degradation efficiency)
Hidden Layers	From 2 to 16
Transfer Function	Tangent sigmoid (TANSIG)
Performance function	Mean Square Error
Data division	70%-15%-15% for training- validation- testing
Data division function	Dividerand
Training function	*Traingdx*

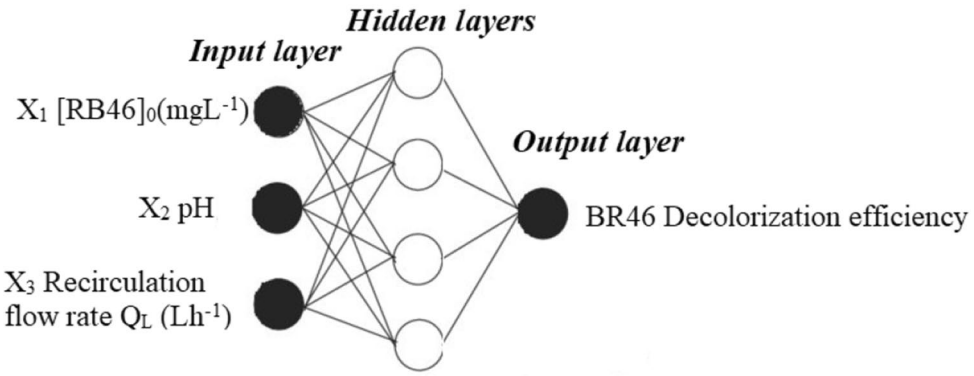

Fig. 2 Neural Network Architecture for input/output variables

in which y_i and $y_{i\text{-pred}}$ are the experimental and predicted values obtained either from ANN or RSM, $y_{i\text{-av}}$ is the average values, and n is the number of experiences.

In the present work, log-sigmoidal and linear transfer functions were used for hidden and output layers, respectively.

3 Results and discussions

3.1 Box-Wilson modeling

The three-level matrix generated by the Box–Wilson design was used for the experimentally obtained responses for photodegradation is shown in Table 5. Based on these results, the empirical relationship that relates the response and selected variables was obtained:

$$\mathbf{Y} = 78.17 - 0.290X_1 + 4.178X_2 - 3.349X_3 - 3.139X_1X_2 - 0.796X_1X_3 + 4.509X_2X_3 - 5.222X_1^2 + 4.669X_2^2 - 0.106X_3^2 \quad (11)$$

The diagnostic plots describes the residual analysis, which is mainly based on the difference between the observed and the predicted response value of the response surface design, thus ensuring that the statistical assumptions fit the analysis data (Fig. 3). Normal probability plots

Table 5 Experimental design matrix, experimental results and predicted photocatalytic decolorization efficiency

Exp	[BR46] (mg L^{-1})	Ph	Flow rate (L min^{-1})	Yield (%)	
				Measured	Predicted
1	− 1	− 1	− 1	77.33	78.62
2	1	− 1	− 1	89.63	87.07
3	− 1	1	− 1	65.52	67.52
4	1	1	− 1	61.00	63.42
5	− 1	− 1	1	80.18	77.89
6	1	− 1	1	85.03	83.15
7	− 1	1	1	82.14	84.83
8	1	1	1	78.70	77.54
9	− 1.68	0	0	65.05	62.91
10	+ 1.68	0	0	61.94	63.88
11	0	− 1.68	0	95.11	98.39
12	0	+ 1.68	0	87.83	84.34
13	0	0	− 1.68	74.05	72.23
14	0	0	+ 1.68	81.88	83.50
15	0	0	0	78.33	78.16
16	0	0	0	78.33	78.16
17	0	0	0	78.33	78.16
18	0	0	0	77.33	78.16
19	0	0	0	78.33	78.16
20	0	0	0	78.33	78.16

of the residuals are a suitable graphical method to verify whether the standard deviations between the actual and the predicted response values follow a normal distribution [16]. The results illustrated in Fig. 3 convey the general impression of a normal distribution of underlying errors since the residuals fall near a straight line; thus, there is no clear indication of non-normality of the experimental results. Based on this plot, the residuals appear to be randomly scattered; thus, the proposed model was adequate, and the constant variance assumption was confirmed.

The experimental responses versus the predicted ones are shown in Fig. 3. The predicted values approximated the observed values in all sets of experiments. Also, there were tendencies toward a linear regression fit. The predicted values agreed well with the experimental data with a coefficient of determination of $R^2 = 0.95$ and adjusted coefficient of determination of $R_{adj}^2 = 0.908$. These results imply that 95% of the variations in percent degradation could be explained by the selected variables. The adjusted R^2 (R_{adj}^2) is a corrected goodness-of-fit parameter, and it was also close to the coefficient of determination R^2, which indicates that the regression predictions accurately approximated the real data points.

3.2 Analysis of variance (ANOVA)

Analysis of variance (ANOVA) was used to determine the important main and interaction effects of factors that influence the dye photodegradation efficiency (Table 6). This model is extremely significant and could be validated by Fisher value (F–value = 21.53), which is greater than the critical F-value at a level of significance $\alpha = 0.95$ (F-tabular = 3.48), indicating that the differences in treatment were highly significant. For statistical significance, we expect the absolute value of the t-ratio to be > 2 or the P-value to be < the significance level ($\alpha = 0.05$). The P-values were also used to verify the significance of each coefficient; if the p-value < 0.05, the terms of model would be significant; thus, the coefficient was more significant with a greater

Table 6 Analysis of variance (ANOVA) for fit of decolorization efficiency from central composite design

Source of variation	Sum of squares	Degree of freedom	Adjusted mean square	F value
Regression	1423.85	9	158.206	21.53
Residuals	73.48	10	7.348	
Total	1497.33	19		

$R^2 = 0.9509$. Adj- $R^2 = 0.9068$. F-value = 21.53» $F_{0.05}$ (9.10) tabular = 3.34

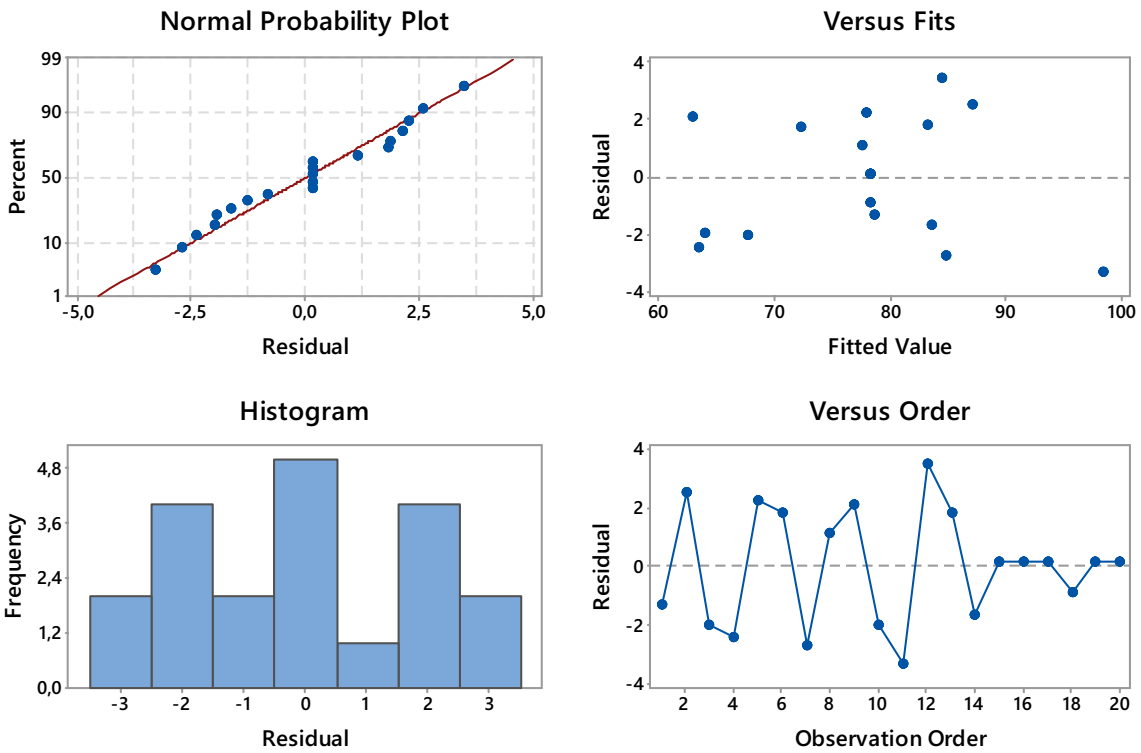

Fig. 3 Residual plots for photocatalytic decolorization efficiency of BR46

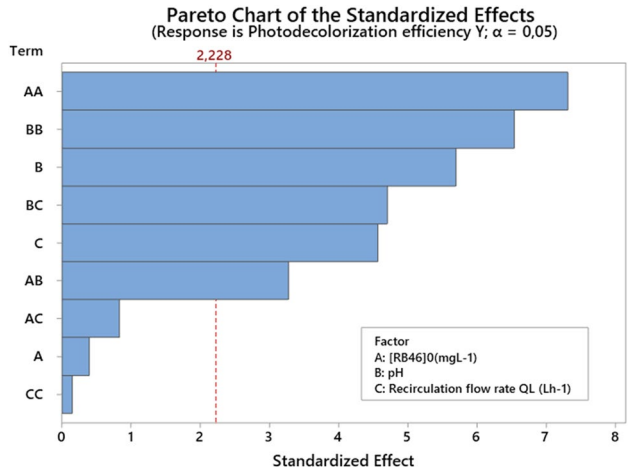

Fig. 4 Pareto chart for BR46 photodecolorization efficiency

Table 7 Regression results from the data of central composite design experiments

Coefficient	Parameter estimate	Standard error	t-value	P-value
a_0	78.16	1.105	70.70	0.000
a_1	0.28	0.73	0.39	0.701
a_2	− 4.17	0.73	− 5.69	0.000
a_3	3.34	0.73	4.56	0.001
a_{11}	− 5.2	0.71	− 7.31	0.000
a_{22}	4.66	0.71	6.53	0.000
a_{33}	− 0.10	0.71	− 0.14	0.885
a_{12}	− 3.13	0.95	− 3.27	0.008
a_{13}	− 0.79	0.95	− 0.83	0.425
a_{23}	4.51	0.95	4.70	0.001

Student's t-test magnitude and smaller *p*-values [30] as shown on the Pareto chart (Fig. 4). It is clear that the main significant reaction parameters followed a specific order (reported as most to least significant): quadratic of dye concentration > quadratic effect pH > effect of pH > interaction between pH and flow rate > effect of flow rate > interaction between initial concentration of the dye and pH.

3.3 Response surface plots effect of factors and interactions on BR46 degradation

The effects of factors can be estimated from the second-order polynomial equation and Student's *t*-test, and synergistic or antagonistic effects correspond to the positive or negative model coefficient.

The Student's *t*-test (Table 7) was used to determine whether the effects differed significantly from zero according to the following relation [15, 31]:

$$t_i = \frac{|ai|}{\sigma i} \tag{12}$$

It is clear from Table 7 that the main significant reaction parameters followed a specific order (reported a most to least significant): second-order effect of initial dye concentration > second-order effect of pH > initial pH > interaction between the flow rate and initial pH > flow rate > interaction between the effect of initial dye concentration and pH.

Response surface and contour plots were generated by stat software (MINITAB 17) to study the effect of interactions of the three variables tested on the decolorization and the degradation efficiency Y (%) as shown in Fig. 5 in which a disc-shaped contour scheme indicates that the interaction between factors was insignificant, while an elliptical form (egg-shaped) designated the importance of the interaction on either side of the selected factors [32, 33]. The results revealed that the decolorization yield Y (%) was more significant at low flow rate and acidic pH within the selected ranges of BR46 concentration while maintaining the reaction time at 150 min in all experiments. This finding could be explained by the fact that the solution is more exposed to solar radiation, which generated more hydroxyl radicals (°OH) and led to increasing degradation efficiency. Also at high flow rates and under alkaline conditions, photodegradation presents very significant results [16]. The presumed reason for that finding is that when the recirculated liquid flow is increased, the turbulence in the system was enhanced, which ensured better dispersion of particles (BR46 and TiO_2) in the solution inside the reactor. Higher decolorization efficiencies at higher flow rates were also attributed to the increase in the mass transfer coefficient [34]. Degradation efficiencies of dyes were observed under alkaline conditions and at higher flow rates, which may have been due to cationic nature of BR46 dye; thus, in basic medium, hydroxyl radicals were produced on the catalyst surface via the reaction shown below:

$$TiO_2\left(h^+_{vb}\right) + OH\,(ads)^- \rightarrow {}^\circ OH \tag{13}$$

High pH favors adsorption on the catalyst surface, which results in high decolorization efficiency [15].

3.4 ANN modeling

The main objective of ANN modeling is to determine the optimal operational conditions (topology) in order to predict BR46 degradation; thus, several topologies were tested by varying the number of neurons in the hidden layer from 2 to 20. The MSE and coefficient of determination (R^2) were used to investigate the relationship between the neurons in the hidden layer and network error, and obtained results are

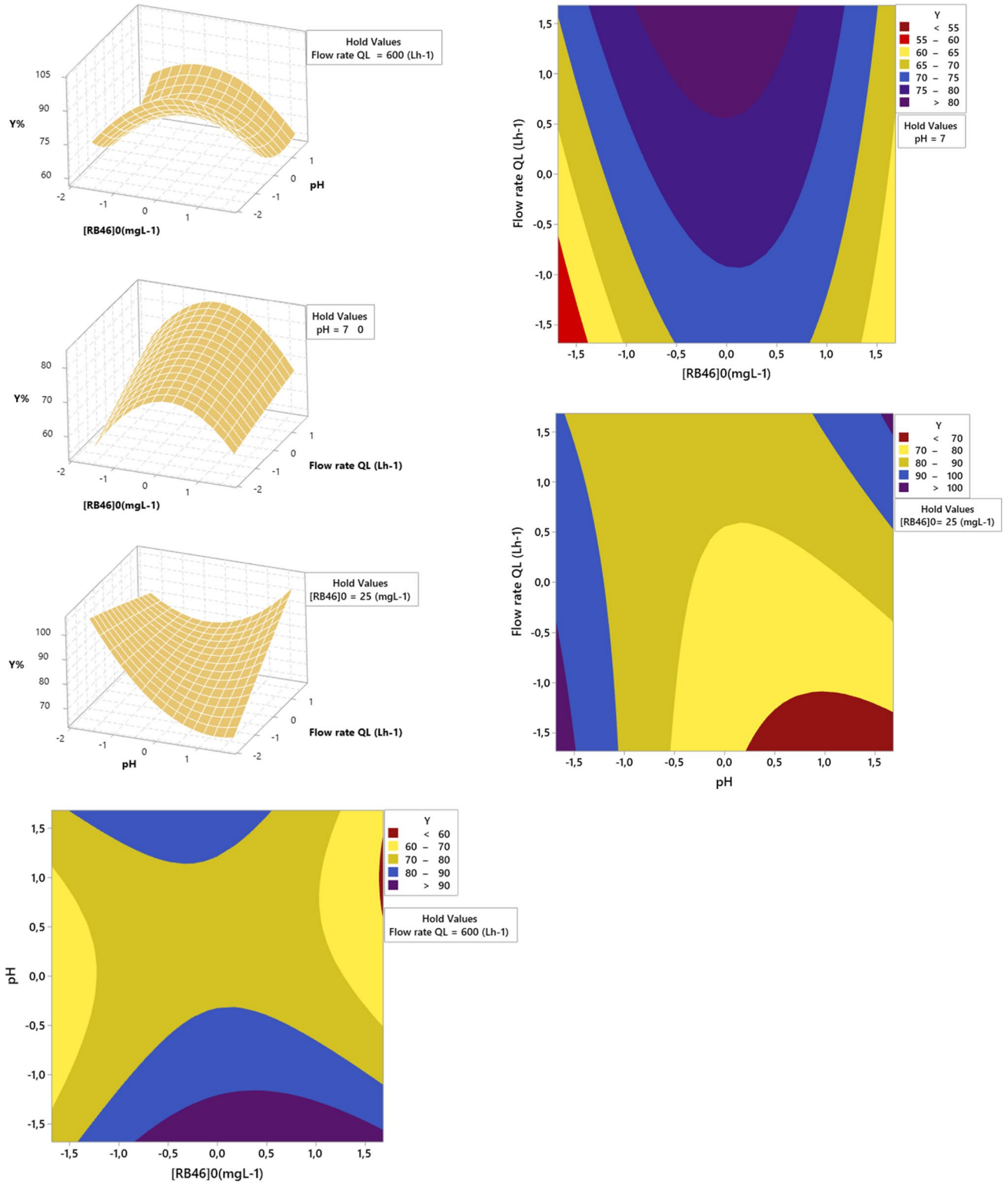

Fig. 5 The response surface and contour plots of photocatalytic degradation efficiency (Y%)

illustrated in Fig. 7a. The findings indicate that the MSE decreased and increased by changing the hidden neuron sizes. Accordingly, the optimal value of the corresponding number of inputs, hidden, and output layers was $3 \times 4 \times 1$, which was selected as the optimum topography to model the BR46 decolorization process. The number of sessions for the

obtaining the best framework was established, and finally, after 897 iterations, the optimal network was achieved. The values of the regression coefficients were 0.9995, 0.9879, 0.9651, and 0.9849 for training, validation, testing (Fig. 6b), and all parameters, respectively. The results indicated that the neural network approximation would perform better for a response that is not "smooth", whereas the classical RSM does not perform well in these types of situations.

3.5 Optimal conditions and plausible mechanism of photodegradation

In order to prove the power of the statistical tool used to optimize the operating conditions of the solar reactor which allowed maximum degradation of the BR46 azo dye; the process of obtaining optimum values for the maximum decolorization efficiency is easily determined by taking the derivatives with respect to each variable asnd solving for zero, and in our case, were 10.65 mg L^{-1} and 10.82 and 852

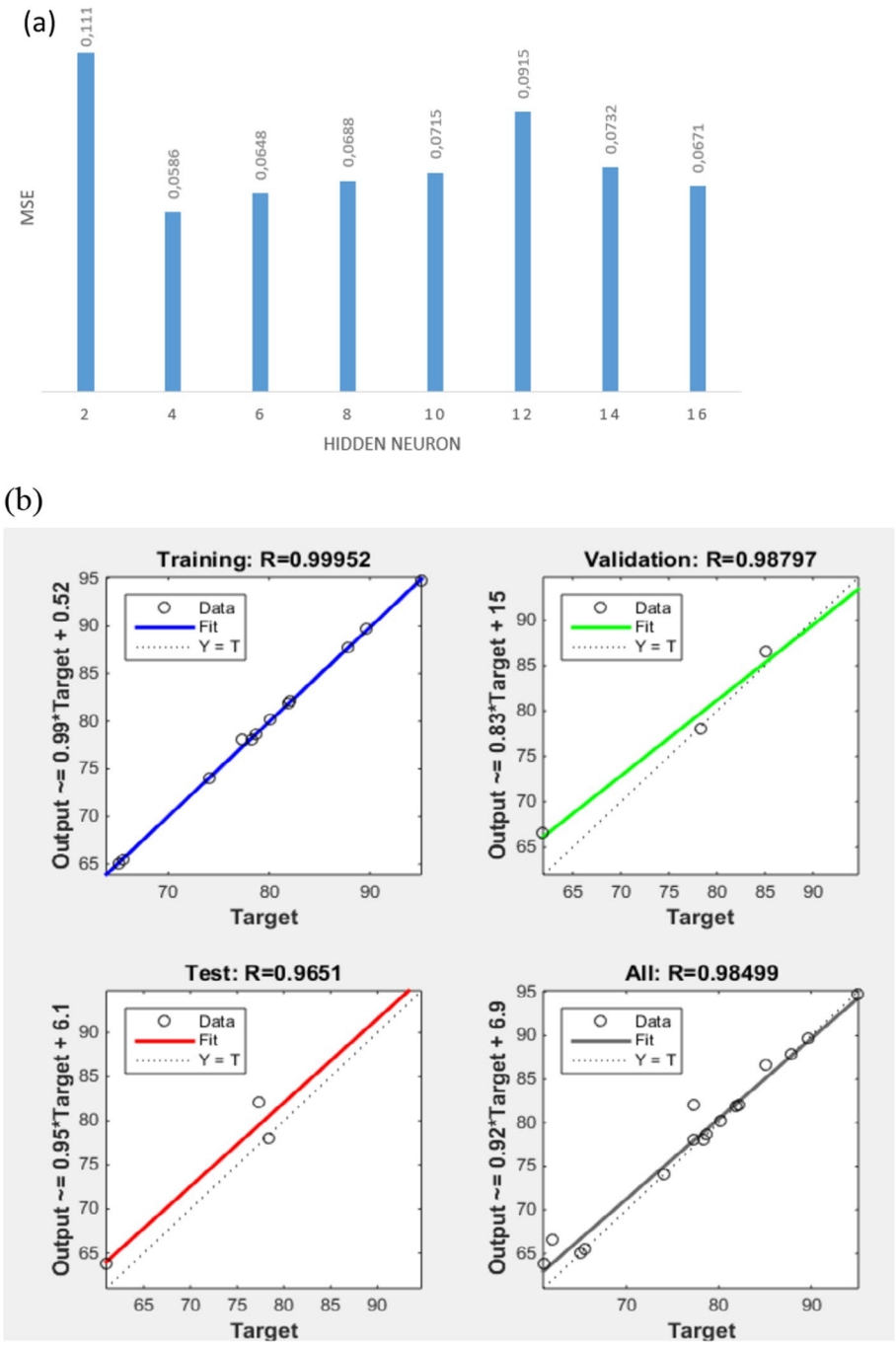

Fig. 6 **a** MSE versus a number of neurons in a hidden layer. **b** Neural network showing the regression analysis of training, validation, and target for photodegradation efficiency of BR46

L h^{-1} for initial dye concentration (X_1), initial pH (X_2), and flow rate (X_3), respectively.

After using additional experimental test to verify the predicted values, the results indicate that the maximal decolorization efficiency was obtained when the values of each parameter were set as the optimum values, which is in good agreement with the predicted value from the regression model. This find implies that the strategy to optimize decolorization conditions and to obtain the maximal decolorization efficiency by RSM for the photocatalytic degradation of the dye Basic Red 46 in this study was successful. Furthermore, this study introduces a way to optimize such a photoreactor and will enable to apply in this device, a specific treatment for a real water obtained from Aurassienne Spinning and Blankets (SAFILCO) Company, Algeria, charged by the dye, C.I. Basic Red 46 to impose the optimal results. The Fig. 7 shows the mechanism of BR46 photodecolorization in the immobilized photocatalyst media. Solar UV light irradiation provides photons with adequate energy, which led to molecular excitation on the surface of TiO_2 resulting in the generation of mobile electrons in the higher energy conduction band and positive holes in the lower energy valence band (Eqs. 1–5). The reactions occur near the TiO_2 surface between electrons as a scavenger of oxygen molecules in order to avoid the electron–hole recombination step, and the holes with adsorbed water allowed for generation of °OH radicals, which eventually degraded the RB46 molecules. The efficiency of the immobilized catalyst could be explained by participation of all of the inner parts of the film in the generation of e − /h + pair the BR46 molecules that were in close enough proximity to the TiO_2 particles [35–37].

4 Conclusion

The response surface methodology and the Box–Wilson design and ANN were used for analysis of the decolorization of the industrial azo-dye, C.I BR46 in a solar photoreactor and to evaluate the individual effects of three independent parameters: initial concentration of the dye, pH and flow rate on photodegradation effectiveness. Analysis of variance (ANOVA) and the ANN approach revealed that predicated models were perfectly fitted with the experimental data giving the highest value of coefficient of determination ($R^2 = 95\%$ and $= 0.999$ for RSM and ANN, respectively) for

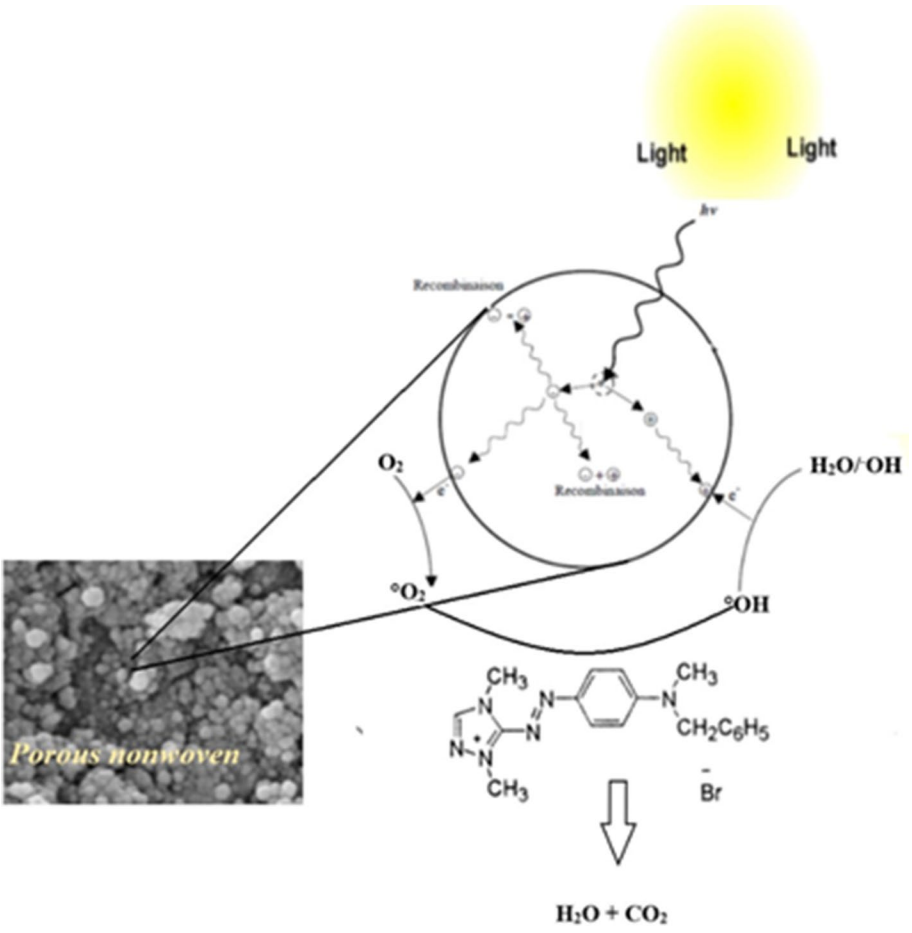

Fig. 7 Plausible mechanism of photodecolorization of BR46 in the immobilized catalyst

optimal topology consisting of the number of input, hidden, and output layers of 3 × 4 × 1, respectively. The optimal conditions found by RSM and ANN were initial concentration of colorant 10.65 mg L^{-1}, pH 10.82, and rate of fluid flow 852 L h^{-1}. The decolorization removal efficiency under these optimal conditions was 99%. Also, we think that such a device is perfectly integrated for a photocatalysis operation and can be easily extrapolated for specific water treatment containing pollutants resistant to conventional treatment.

References

1. Lelli B, Fávaro-Polonio CZ, Pamphile JA, Polonio JC (2019) Effects of textile dyes on health and the environment and bioremediation potential of living organisms. Biotechnolo Res Innov 3(2):275–290
2. Sillanpää M, Ncibi MC, Matilainen A (2018) Advanced oxidation processes for the removal of natural organic matter from drinking water sources: a comprehensive review. J Env Manag 208:56–76
3. DEPA (Danish Environmental Protection Agency) (2000) Survey of azo-colorants in Denmark, Toxicity and fate of azo dyes, Danish Technological Institute, Environment. DEPA (Danish Environmental Protection Agency), Copenhagen
4. Opie J, Adriene L, Kathryn F, John F, Rosemary N (2004) Foot dermatitis caused by the textile dye Basic Red 46 in acrylic blend socks. Contact Dermatitis 49:297–303
5. González-Casamachin DA, De la Rosa JR, Lucio-Ortiz CJ, De Rio DADH, Martínez-Vargas DX, Flores-Escamilla GA, Moctezuma-Velazquez E (2019) Visible-light photocatalytic degradation of acid violet 7 dye in a continuous annular reactor using ZnO/PPy photocatalyst: synthesis, characterization, mass transfer effect evaluation and kinetic analysis. Chem Eng J 373:325–337
6. Isimjan TT, Trifkovic M, Abdullahi I, Rohani S, Ray AK (2015) Nanoscale optimization and statistical modeling of photoelectrochemical water splitting efficiency of N-doped TiO_2 nanotubes. Top Cata 58(2–3):114–122
7. Da Silva CG, Faria JL (2003) Photochemical and photocatalytic degradation of an azo dye in aqueous solution by UV irradiation. J Photochem Photobiol A Chem 155:133–143
8. Li W, Jain T, Ishida K, Liu H (2017) A mechanistic understanding of the degradation of trace organic contaminants by UV/hydrogen peroxide, UV/persulfate and UV/free chlorine for water reuse Environmental Science. Wat Res Technol 3(1):128–138
9. Glover JD, Hartley AC, Windmiller RA, Nelsen NS, Boyd JE (2018) An overview of solar photocatalytic reactor designs and their broader impact on the environment visible light-active photocatalysis: nanostructured catalyst design. Mech Appl. https://doi.org/10.1002/9783527808175.ch20
10. Spasiano D, Marotta R, Malato S, Fernandez-Ibanez P, Di Somma I (2015) Solar photocatalysis: materials, reactors, some commercial, and pre-industrialized applications A comprehensive approach. App Catal B: Environ 170:90–123
11. McCullagh R, Peter KJ, Adams M, Pollard PM, Abdurrahman M (2010) Development of a slurry continuous flow reactor for photocatalytic treatment of industrial waste water. J Photochem Photobiol A Chem 211:42–46
12. Buechler KJ, Nam CH, Zawistowski TM, Noble RD, Koval CA (1999) Design and evaluation of a novel controlled periodic illumination reactor to study photocatalysis. Ind Eng Chem Res 38:1258–1263
13. Sacco O, Sannino D, Vaiano V (2019) Packed bed photoreactor for the removal of water pollutants using visible light emitting diodes. App Sci 9(3):472
14. Montalvo-Romero C, Aguilar-Ucán C, Ramirez-Elias M, Cordova-Quiroz V (2018) A semi-pilot photocatalytic rotating reactor (RFR) with supported TiO_2/Ag catalysts for water treatment. Molecules 23(1):224
15. Bouchareb MK, Bouhelassa M, Berkani M (2014) Optimization of photocatalytic decolorization of CI Basic Blue 41 in semi-pilot scale prototype solar photoreactor. J ChemTechnol Biotechnol 89:1211–1218
16. Berkani M, Bouhelassa M, Bouchareb MK (2019) Implementation of a venturi photocatalytic reactor: optimization of photodecolorization of an industrial azo dye. Ara J Chem 12(8):3054–3063
17. Chen LC (2000) Effects of factors and interacted factors on the optimal decolorization process of methyl orange by ozone. Wat Res 34:974–982
18. Oppenlander T (2003) Photochemical Purification of Water and Air. Wiley, Weinheim
19. Radha KV, Sirisha K (2018) Electrochemical oxidation processes. Advanced oxidation processes for waste water treatment. Academic Press, Cambridge, pp 359–373
20. Balkin SD, Lin DK (2000) A neural network approach to response surface methodology communications in statistics. Theor Methods 29(9–10):2215–2227
21. Elmolla ES, Malay C (2011) The use of artificial neural network (ANN) for modelling, simulation and prediction of advanced oxidation process performance in recalcitrant wastewater treatment. Artif Neural Netw Appl. https://doi.org/10.5772/14920
22. Strik DP, Domnanovich AM, Zani L, Braun R, Holubar P (2005) Prediction of trace compounds in biogas from anaerobic digestion using the MATLAB Neural Network Toolbox. Environ Modell Softw 20(6):803–810
23. Azadi S, Karimi-Jashni A, Javadpour S (2018) Modeling and optimization of photocatalytic treatment of landfill leachate using tungsten-doped TiO_2 nano-photocatalysts: application of artificial neural network and genetic algorithm. Process Saf Environ Prot 117:267–277
24. Dhiman N, Singh A, Verma NK, Ajaria N, Patnaik S (2017) Statistical optimization and artificial neural network modeling for acridine orange dye degradation using in-situ synthesized polymer capped ZnO nanoparticles. J Colloid Interface Sci 493:295–306
25. Khataee A, Fathinia M, Zarei M, Izadkhah B, Joo S (2014) Modeling and optimization of photocatalytic/photoassisted-electro-Fenton like degradation of phenol using a neural network coupled with genetic algorithm. J Ind Eng Chem 20(4):1852–1860
26. Ayodele BV, Alsaffar MA, Mustapa SI, Vo DVN (2020) Back-propagation neural networks modelling of photocatalytic degradation of organic pollutants using TiO_2-based photocatalysts. J ChemTechnolo Biotechnolo. https://doi.org/10.1002/jctb6407
27. Talwar S, Verma AK, Sangal VK (2019) Modeling and optimization of fixed mode dual effect (photocatalysis and photo-Fenton) assisted Metronidazole degradation using ANN coupled with genetic algorithm. J Environ Manag 250:109428
28. Khataee AR, Fathinia M, Aber S, Zarei M (2010) Optimization of photocatalytic treatment of dye solution on supported TiO_2 nanoparticles by central composite design: intermediates identification. J Hazard Mater 181(1–3):886–897
29. Ko S (2008) Zeolite-based nanosized TiO2 photocatalytic paper for antimicrobial barrier and toxin passivation in packaging: design, synthesis and characterization. Dessertation. Western Michigan University, Kalamazoo
30. Liu HL, Chiou YR (2005) Optimal decolorization efficiency of Reactive Red 239 by UV/TiO_2 photocatalytic process coupled with response surface methodology. Chem EngJ 112:173–179

31. Jasso-Salcedo AB, Hoppe S, Pla F, Escobar-Barrios VA, Camargo M, Meimaroglou D (2017) Modeling and optimization of a photocatalytic process: degradation of endocrine disruptor compounds by Ag/ZnO. Chem Eng Res Des 128:174–191
32. Kesraoui-Abdessalem A, Oturan N, Bellakhal N, Dachraoui M, Oturan MA (2008) Experimental design methodology applied to electro-Fenton treatment for degradation of herbicide chlortoluron. Appl Catal B 78:334–341
33. Berkani M, Bouhelassa M, Bouzaza A, Bouchareb MK, Kadmi Y, Soutrelle I (2015) Optimization of photocatalytic decolourization of cationic Azo Dye in thin film fixed bed photoreactor. Chem Eng. https://doi.org/10.3303/CET1543161
34. Rabahi A, Hauchard D, Arris S, Berkani M, Achouri O, Meniai AH, Bencheikh-Lehocine M (2018) Leachate effluent COD removal using electrocoagulation A response surface methodology (RSM) optimization and modelling. Desalin Wat Treat 114:1–12
35. Dijkstraa MFJ, Pannemana HJ, Winkelmana JGM, Kellyb JJ, Beenackers AACM (2002) Modeling the photocatalytic degradation of formic acid in a reactor with immobilized catalyst. Chem Eng Sci 57:4895–4907
36. Hir ZAM, Moradihamedani P, Abdullah AH, Mohamed MA (2017) MA Immobilization of TiO_2 into polyethersulfone matrix as hybrid film photocatalyst for effective degradation of methyl orange dye. Mat Sci Semicon Proc 57:157–165
37. Danion A, Bordes C, Disdier J, Gauvrit J-Y, Guillard C, Lantéri P, Jafrezic-Renault N (2004) Optimization of a single TiO_2-coated optical fber reactor using experimental design. J Photochem Photobiol A 168(3):161–167